International Journal of Emerging Trends & Technology in Computer Science (IJETTCS)
Web Site: www.ijettcs.org Email: editor@ijettcs.org, editorijettcs@gmail.com
Volume 9, Issue 5, September - October 2020 ISSN 2278-6856

Verification and validation of a finite element model of a human-powered vehicle chassis

Carlos Urrego[1] and Uriel Zapata[2]

[1]Department of Mechanical Engineering, EAFIT University, Medellin, Colombia.

[2]Department of Mechanical Engineering, EAFIT University, Medellin, Colombia.

Abstract: ***The aim of this study was to evaluate the impact of verification and validation processes in the predictive precision and accuracy of a finite element model of a human-powered vehicle (HPV) chassis. The three-dimensional (3D) geometry of a steel frame structure was obtained using a 3D laser scanner to create a static finite element model of the structural system. Static operational loading conditions were physically represented using hollow concrete blocks and subsequently simulated in the software SolidWorks. Basic boundary conditions were applied to the physical model in order to ensure structural stability and resemble real-world settings. The verification and validation processes were developed according to the Guide for Verification and Validation in Computational Solid Mechanics from the American Society of Mechanical Engineers. The verification process was performed through a sensibility analysis, in which the model was subsequently re-meshed by increasing the number of elements until output values converged. The validation process was performed by comparing the computational model's stress and strain outputs with the corresponding quantitative values obtained from a strain gauge located in the physical model; the strain distribution of one part of the model was compared with that obtained using a photo-elastic technique. It was found that 716,890 was an acceptable number of solid tetrahedral elements needed to guarantee reliability in the HPV model outputs. In addition, the relative error between the experimental outputs and the computational model was 0.13% for normal principal stress and 3.73% for normal principal strain. These findings make clear that the processes of validation and verification are essential for quantifying the uncertainties and evaluating the predictive capacities of computational models of physical structures.***

Keywords: Static analysis, mechanical design, structure, uncertainty, accuracy, precision.

1. INTRODUCION

Computer simulation of mechanical systems can be performed by finite element analysis (FEA) in order to quantitatively predict the design performance and safety of engineered structures [1]. As a powerful engineering tool that provides an alternative solution to traditional analytical methods, FEA is used to examine a wide variety of physical situations in a broad range of fields such as mechanical design, civil engineering, electric engineering, and biomedical engineering [2]-[5]. The calculations performed by the FEA are based on a numerical technique developed to solve partial differential equations, solving massive problems by discretizing them [6]-[7].

Users of the finite element method often assume that the careful fulfillment of the pre-processing, solving, and post-processing phases is sufficient for obtaining reliable results [8]. However, the finite element method involves not only systematic and random errors but also several uncertainties that potentially compromise the accuracy and precision of the predicted results from FEA [9]. The uncertainties in the computational model can be present in (1) the geometrical parameters of the model, (2) the loading conditions of the model, (3) the material properties assigned to the model, and/or (4) the selected boundary conditions that constrain the physical response of the model. Moreover, both systematic and random errors are associated with specific FEA methods [10].

Verification, also known as convergence testing, is the process of searching for numerical precision in order to reduce error. This process checks whether the computational model truly represents the mathematical model and its solution [11]. Thus, the convergence test aims to remove the error of the computational model by building an asymptotic solution using a sequence of repeated finite element models. Complementarily, the validation process quantifies the uncertainties in order to assess the degree of accuracy with which the computational models predict the real physical outputs from the perspective of the planned uses of the model [10].

The implementation of verification and validation (V&V) processes is always needed in order to increase the FEA's predictive confidence for producing quantitative outputs whose representativeness encompasses not only reliability (i.e., precision) but also validity (i.e., accuracy). As stated in the literature, V&V methodology should always begin with the verification process, which evaluates the precision of the FEA output [12], followed by the validation process, which determines the degree of accuracy that a FEA possesses in its representation of the physical model [13]. In sum, V&V is a complementary methodology intended to increase both the precision and the accuracy of the quantitative predictions in the computational model outputs [14].

Engineering design often involves complex structures, for whose analysis a hierarchical study must be performed, starting from the main component. For vehicles, the chassis is the frame part or basic structure that endures the stresses and deformations that result from operational conditions for which the chassis is designed [15]-[16]. In addition, it is the

main structure to which all the other functional and non-functional components are attached [16]. In a human-powered vehicle (HPV), the following components are mounted in the frame: suspension, seat, wheels, transmission system, handlebar, and anti-roll cage. Each of these attachments serves in some way as a load input or fixture for the structural system [15].

Few meta-analytic studies of computational models have been undertaken to evaluate the incidence of V&V processes. Thus, many flawed FEA models with unmeasured uncertainties may not truly represent the intended reality, leading to erroneous conclusions and inferences related to the analyzed designs [17]. In the engineering field, inconsistent conclusions involving high-impact decisions may lead to failure of systems [8], [18]. The objective of this study is to evaluate the impact of V&V processes in a FEA of a HPV chassis. We operate under the axiom that FEA can accurately predict stress and strain values not only with validity, but also with reliability.

2. MATERIALS AND METHODS

The subject of study was a chassis made of 1.5 inches diameter tubular 1020 steel with 2.1mm average wall thickness and a 76.59GPa Elastic Modulus and 230MPa of Yielding Stress (Figure 1; Table I), with an average weight of 116.15 N and global dimensions as follows: 1,417 mm in length, 678 mm in height, and 470 mm in width. The structural system was analyzed under certain loading conditions that represented the operational situations of the frame structure. The operational loads were simulated using concrete bricks of the following weights: (1) 60.822 N, (2) 68.278 N, (3) 65.433 N, (4) 68.0814 N, (5) 184.624 N, (6) 176.188 N, (7) 111.638 N, (8) 110.166 N, (9) 66.512 N, and (10) 67.787 N (Figure 2). Furthermore, three car jack stands used as supports provided the necessary stability to the structural system and represented the desired boundary conditions.

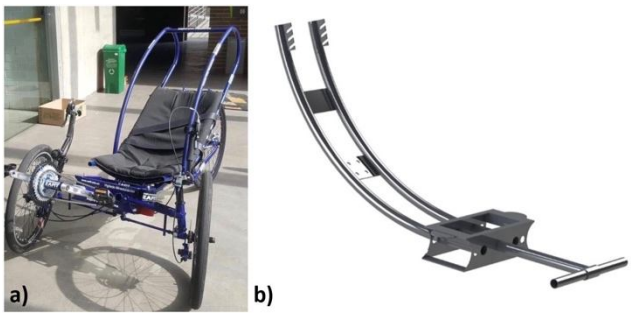

Figure 1(a) Human-powered vehicle (HPV) and (b) Mainframe of the chassis used for the HPV

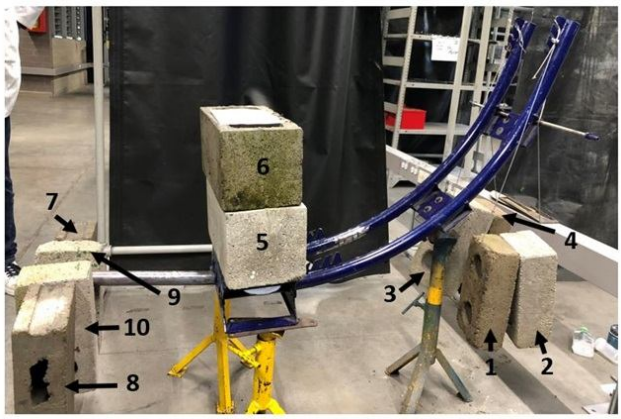

Figure 2 HPV physical model loaded with bricks simulating the operational critical load condition

2.1 3D Scan

A reverse-engineering process was used to create a 3D geometrical model of an existing physical frame [19]. The 3D geometries of all the structural components of the HPV chassis were digitized using a high-precision infrared laser scanner (HandyScan 700; Creaform, Levis, Canada) [20]. Positioning targets (Creaform, Levis, Canada) were placed on the surface of the HPV in order to provide the required static reference system for the laser scanner. A total of 205 black contour positioning targets of 6 mm in diameter were directly placed on the physical model, with an average distance of 50 mm between nearest neighbors.

Prior to placing the positioning targets, the whole chassis of the HPV was covered with a matte-finish paint in order to reduce the light reflection that would distort the laser scans. The scanning parameters for the laser scanner were as follows: 0.2-mm resolution, 2.54-ms shutter speed, and 0.30-m average distance between the scanner and the chassis. The chassis was scanned in the two following steps: first, the structure was scanned while supported in a position resembling the condition as it would normally operate; next, after completing the mesh scanning, the structure was turned upside-down in order to reach the zone of the model that was inaccessible in the first configuration, so as to cover the whole structure's surface.

The scanning process was performed in a dust-free environment under controlled conditions with an average room temperature of 25°C and an average relative humidity of 64%, all the latter environmental conditions meet the requirements for the optimal function of the scanner. During the scanning process, the laser scanner was moved around the metallic frame of the HPV, collecting 550,000 measurements per second. The mesh database, based on the captured point cloud, was imported to a workstation (ZBook, 64 GB memory, Intel Core i7 processor, Navidia QUADRO; HP), using the scanner's post-processing software (VXElements, Ver. 6.3SR1; Creaform).

Once the point cloud mesh of the physical model was obtained, post-processing proceeded using Geomagic Design X software (Ver. 2018; 3D Systems, Rock Hill, SC, USA) to reconstruct the missing information, remove noise, and improve the mesh [21]. After obtaining a completely closed mesh, the model was exported to Geomagic Control

X software (Ver. 2018; 3D Systems) to provide a deviation analysis between the scanned and the reconstructed geometries. Finally, the mesh was exported to the FEA software SolidWorks (Ver. 2018; DassaultSystémes, Vélizy-Villacoublay, France) and was converted into a solid model (Figure 3).

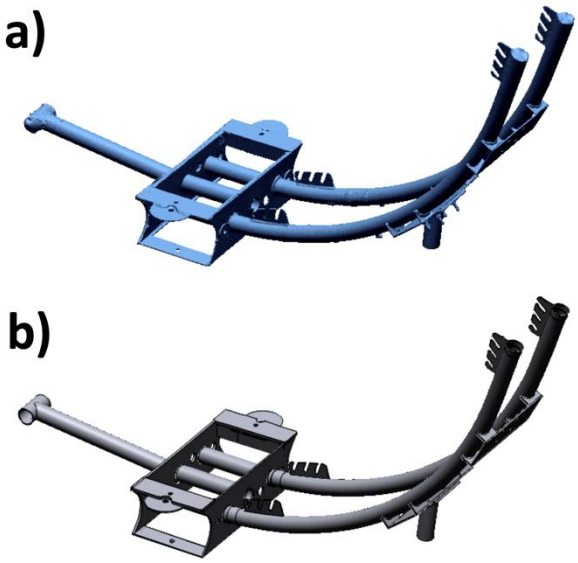

Figure 3 (a) 3D-scanned model in Geomagic Design X software. (b) 3D-solid geometry imported into Solidworks software, ready for simulation using finite element analysis

2.2 Finite Element Model

Using the reconstructed geometry of the scanning process of the components of the HPV, a 3D geometrical FEA model was imported to the software SolidWorks (Ver. 2018; DassaultSystémes). The mechanical properties of the material used for the construction of the physical model were defined according to specifications provided by the local supplier (Table I), which were applied to all the components of the numerical model for the FEA simulation.

Table 1: Mechanical properties of the material used for the FEA model of the HPV structure

Property	Value	Units
Elastic Modulus	76.59	GPa
Poisson Ratio	0.29	-
Shear Modulus	75	GPa
Mass Density	7900	kg/m^3
Tension Limi	306	MPa
Yield Strength	230	MPa

The computational model was an assembly composed of several structural components bonded to behave as a single structural system representing the physical design of the chassis, said elements were bonded using the merging tool of Geomagic Design X software prior exporting it to Solidworks. More than 800,000 solid tetrahedral elements with four nodes each were used to create the 3D mesh of the FEA model of the HPV structure. The loads were applied to the surfaces in a way that best resembled the original operational load conditions, using hollow concrete bricks. Moreover, the self-weight of the frame was included within the analysis by multiplying the mass by gravity (9.81 m/s2). The boundary conditions of the model were defined not only to mimic the original structure but also to provide the required statical stability to the system (Figure 4). The vertical displacement was set as zero for all the surfaces where the model was supported in direct contact: also, rotation and lateral displacement were constrained since the real-world physical conditions determined such restrictions.

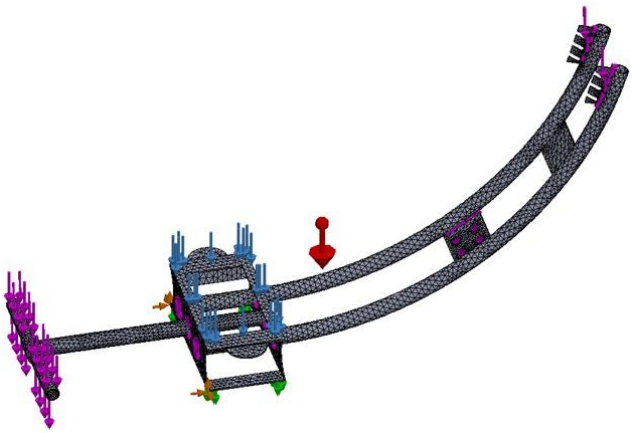

Figure 4 3D model within the FEA software with the material applied, initial meshing, boundary conditions defined, and loads applied. The color convention in the graph is as follows: magenta for anterior and posterior loads, pink and green for displacement restrictions, blue for central load, and red for gravity load exerted on the model

2.3 Verification

The verification process was performed by evaluating the sensibility of the model outputs to different mesh sizes, aiming to determine the minimum number of elements that guaranteed accuracy in the model through a convergence analysis of the mesh [22]. The mesh type used for all the analyses was a combined mesh based on curvature, with four-node tetrahedral elements of a maximum initial size of 15 mm, for a total of 23,363 elements in the first analysis. The criterion of inclusion for the simulations was that the total percentage of elements with an acceptable aspect ratio (<3) was greater than 95%, aiming to achieve an error below the 5% within the software prediction and the measured values.

Eight simulations were performed, with each subsequent simulation built using a reduced maximum element size and thus an increased number of elements. For the final analysis, the mesh characteristics corresponded to a maximum element size of 2.8 mm with a total of 868,828 elements. The principal normal stress (P1) was chosen as

the critical factor for analyzing the convergence procedure, with the output read at the same node in all cases. To analyze the convergence of the values and the sensibility of the model, how the outputs changes when varying the mesh size, the P1 result of each simulation was plotted against the number of elements.

2.4 Validation

A 45º strain gauge rosette (Pattern: 120CZ Model; Vishay Precision Group, Malvern, PA, USA) was placed in the upper part of the left curved structure (Figure 5), and the values of three normal strains were recorded using electronic equipment and LabVIEW software (SCXI-1000 chassis, SCXI modules; National Instruments, Austin, TX, USA). Next, principal normal strain was calculated using Equations 1 and 2, and the stress was calculated using equation 3. Moreover, the frontal plate was evaluated with photo-elastic techniques that have been found suitable for similar situations [23]-[24]. The HPV chassis was covered with PS1 sheet and PC10 adhesive so that the normal strain distribution could be obtained using a PhotoStress® Analysis (Vishay Precision Group). During the test, images were captured using a camera for later comparison with the FEA software results.

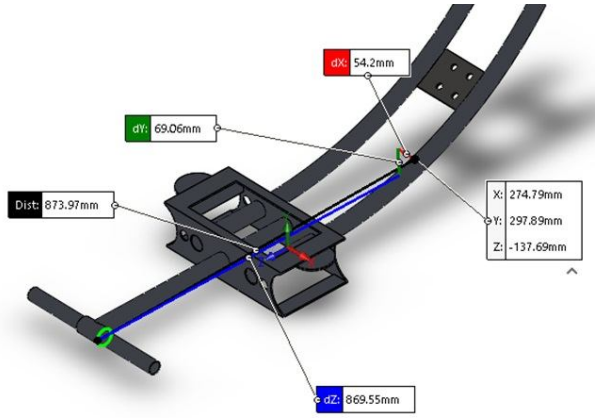

Figure 5 Position of the point of analysis with respect to the frontal tube end; relative coordinates are with respect to the global coordinate system. Overall distance is in black, while the component distances parallel to the X-, Y-, and Z-axes are respectively labeled in red, green, and blue

In order to avoid bias, and increase the present study's confidence level, the finite element model simulation was performed before the laboratory tests and measurements [11]. Complementarily, the validation process was performed by a third party with the intention of reducing bias. The loads were placed smoothly in order to avoid impact and possible flawed data recording or damage to the strain gauge or the photo-elastic coating (Figures 3 and 6). After the load was fully placed, the strain gauge measurements were performed, and the images were taken for the photo-elasticity analysis.

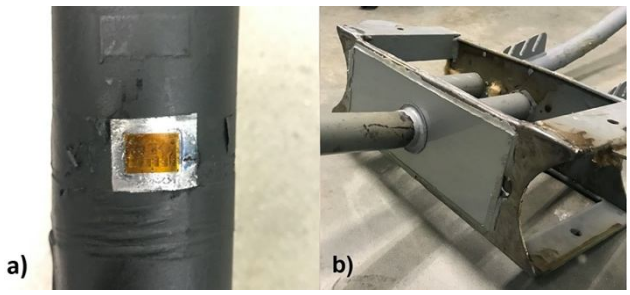

Figure 6 Installation process of (a) rosette and (b) photo-elastic plate used in the validation of the HPV structure

3. RESULTS

3.1 Scanning Process

The two-step process used for scanning the physical chassis proved to be suitable for an adequate geometric reconstruction. Intervention tasks during post-processing were minimal because the mesh result of the scanned model was almost fully closed. This result is attributed to a well-placed reference system that allowed coverage of all parts of the model, as well as to the matte-finish painting that reduced laser reflection, thus increasing the scanning speed by capturing more data and reducing the noise recorded by the equipment.

The use of a high-precision laser scanner increased the level of detail of the obtained geometry while also capturing complex geometries at the welded joints and superficial irregularities attributed to the painting process. In order to ensure that the reconstructed geometry satisfies deviation tolerances, the surfaces serving as references for loads and boundary conditions must be represented as regular or mono-surface entities via a reconstruction process; this mesh must be compared with the original scanned mesh. Deviation analysis was performed by comparing both geometries in Geomagic Control X software with the purpose of evaluating the reconstruction results (Figure 7). In this process, a satisfactory result was obtained in which the reconstructed geometry showed an average deviation of 0.338 mm with respect to the scanned geometry.

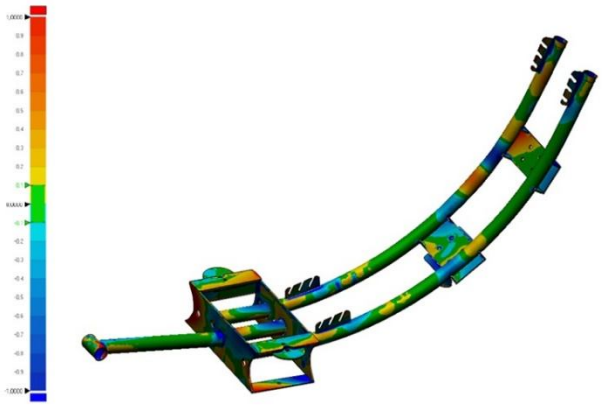

Figure 7 Deviation analysis of the reconstructed mesh with scale in mm. Regions extending beyond the original scanned geometry are marked in red while regions lying below the original geometry are marked in blue. In both

cases, marginal reconstructed mesh values deviated less than 1 mm from the original mesh

3.2 Finite Element Model

The results of the FEA, in terms of stresses, strains, and deformations, were obtained from the 3D structure simulation using SolidWorks software. The principal normal stress pattern (P1) showed a tensional prevalence of stresses at the joint between the frontal plate and the frontal tube with values between 32 and 200 MPa (Figure 8a). These values were 13% lower than the normal yield stress of the material. The principal shear stress (P1−P3/2) showed concentrated levels between 21 and 62 MPa at certain areas along the joints between the plates and tubes of the physical structures (Figure 8b). The maximum principal shear stress value was 73% lower than the shear yield stress of the material.

Furthermore, the pattern of deformations was in accordance with the applied loads. A maximum vertical deformation (uY) of 0.47 mm was found at the anterior part of the physical model, with a secondary maximum of 0.36 mm at the posterior part of the metallic frame (Figure 8c). The lateral part of the physical model showed minimal vertical deformation. The normal principal strains (ε1), as a measurement of the variability of the normal deformations, were comparable with the principal normal stress distribution (Figure 8d). Values between 3 × 10−4 and 1 × 10−6 were detected in the FEA model, identifying the higher magnitude in the zone surrounding the frontal hole of the joint between the plate and the tube.

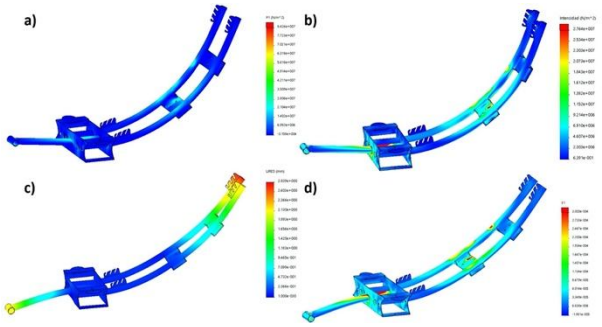

Figure 8 Finite element model outputs: (a) Principal normal stress distribution. (b) Principal shear stresses. (c) Maximum deformations. (d) Principal normal strain distribution

3.3 Verification

The mesh refinement process and its subsequent sensibility analysis were performed to ascertain the accuracy of the structural frame of the HPV. A node, located in the corner of the left side in the central box of the chassis, was selected to read the outputs of the finite element model at a consistent location (Figure 9a). The first principal normal stress (P1) was plotted against the number of elements; this latter variable ultimately proved to be inversely proportional to the element size. Eight simulations were performed, sequentially reducing the element size of the FEA mesh. Convergence of the output was reached at around 450,000 elements (Figure 9b).

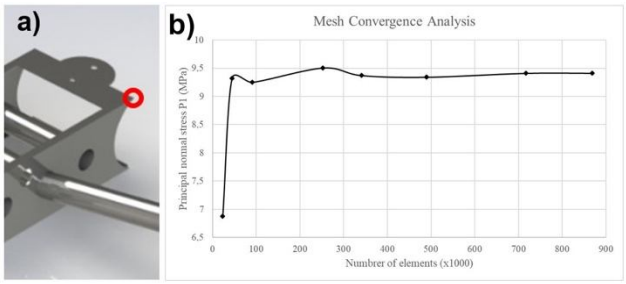

Figure 9 (a) Node of analysis for the verification process and (b) mesh convergence test results

3.4 Validation

Stress and strain measurements were performed within the finite element model using the probe tool at the location of the physical strain gauge (Figure 5), which was created in the software as a reference for reducing the average error in the measurement process. A value of 9.37 MPawas reported for principal normal stress (P1), 1.128×10^{-4} for principal normal strain. The measurement of strain and the prediction of stress in the physical model were performed at the same location as in the numerical model. The strain gauge reported three values as follows:$\epsilon_a=63 \times 10^{-6}$, $\epsilon_b=123 \times 10^{-6}$, and $\epsilon_c=53 \times 10^{-6}$(Figure 10).

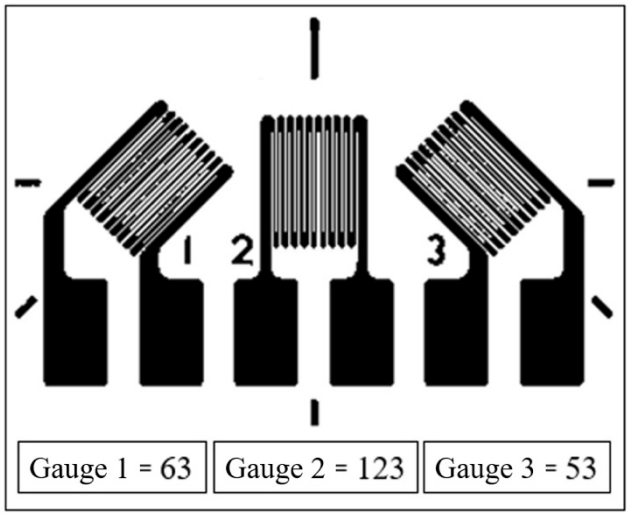

Figure 10 Strain gauge lecture for the validation test in LabVIEW software

$$\epsilon_a=\epsilon_x \cos^2\theta_a+ \epsilon_y \sin^2\theta_a+ \gamma_{xy}\sin\theta_a\cos\theta_a$$
$$\epsilon_b=\epsilon_x \cos^2\theta_b+ \epsilon_y \sin^2\theta_b+ \gamma_{xy}\sin\theta_b\cos\theta_b \quad (1)$$
$$\epsilon_c=\epsilon_x \cos^2\theta_c+ \epsilon_y \sin^2\theta_c+ \gamma_{xy}\sin\theta_c\cos\theta_c$$

where $\epsilon_x=6.3 \times 10^{-5}$,$\epsilon_y=5.3 \times 10^{-5}$ and $\gamma_{xy}=-1.3 \times 10^{-4}$.

$$\epsilon_{principal} = \frac{\epsilon_x+\epsilon_y}{2} + \sqrt[2]{(\frac{\epsilon_x-\epsilon_y}{2})^2 + (\frac{\gamma_{xy}}{2})^2} \quad (2)$$

From this expression, we obtain $\epsilon_1 = 1.238 \times 10^{-4}$

$\sigma_{max} = \epsilon_1 \times E$
(3)

From this expression, we obtain $\sigma_{max} = P1 = 9.36$ MPa.

A complementary photo-elasticity validation process was performed during the test. The images obtained from the physical model were compared with the results in the FEA model by performing a qualitative similarity comparison of the strain distributions of the numerical model and the photo-elastic coating (Figure 11). The distribution of the numerical prediction agreed with the physical model result, but a number of noise factors and threat variables were identified, such as inhomogeneous adhesion between the coating and the plate and insufficient area covered by the coating. Optical noise attributed to the adhesive was also observed, since where the coating ends were fixed by only adhesive without the photo-elastic plate, some results could not be assessed.

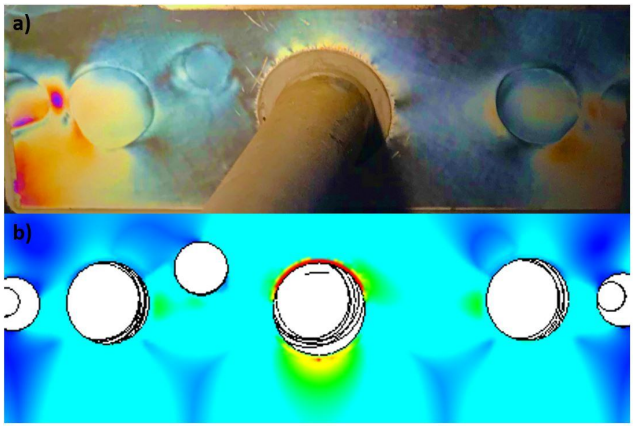

Figure 11 Similarity between (a) the numerical model results for strain distribution and (b) the photo-elastic physical stress patterns

The FEA model displayed the highest strain results near the central hole of the frontal plate. Elevated concentrations of normal principal stresses were found around the lateral holes. High strain values were found under the central hole, though the highest strain values in the model were found in the immediate vicinity of the joint in the upper zone, 3×10^{-4} (Figure 8d). In spite of all this, the overall central strain distributions of both models agree. In contrast to the computational prediction, the photo-elastic coating showed the highest strain values in the lateral bottom corners and around the center plate (Figure 11), exhibiting higher magnitudes near the supports instead of near the joint of the central plate and frontal tube. The strain near this joint could not be assessed since a significant surrounding area was required for gluing the coating to the plate.

The differences between the predictions of the numerical model and the measured values in the physical model were expressed as percentage differences, resulting in an average difference between FEA outputs and laboratory test values of 0.13% for the stress and 3.73% for the strain. Since quantification was based on only one lab test, estimation of statistical variability was not possible.

4. DISCUSSION

Computational models are built with the purpose of making predictions of the engineering responses of physical models. However, the bridge between the computational model and the physical model is based on both precision and accuracy; together, these reflect the strength of the predictions, placing the outputs of both models as near to one another as possible [25]. The quality of the results and the strength of the predictions are improved by reducing the uncertainties, which in turn is accomplished by properly representing the geometry, the materials, the loading patterns, and the boundary conditions in the model [14]. Because the stress prediction results were closer to the real-world values (0.13% difference) than the strain prediction results, which were themselves quite close (3.73% difference), we can accept the hypothesis that the model predicts stress and strain values similar to those of the physical model. Although the stress value predictions are almost thirty times more precise than the strain value predictions, both predictions are below the 5% error tolerance threshold.

The FEA model of the HPV frame showed a minimum overstrength of 30 MPa. However, the studied vehicle's chassis design showed noticeable stress concentration zones corresponding to short-scale transitions in geometric shape. In addition, the highest stress values within the whole system (200 MPa) were exhibited by the central box element and its joints with longitudinal components. This location corresponds to welded joints with mechanical behavior disturbed by thermal stress [26]. In spite of the high stress magnitude patterns, showing a maximum normal principal stress of 30 MPa below the yield limit of the material, the HPV chassis reported only small deformations. This phenomenon may indicate a low dissipation of energy through strain when bearing loads; this dissipation factor may be critical under cyclic loading conditions or in case of a vehicle collision [27].

The material exhibited an unusual low elastic modulus, being an average 60% below the expected behavior; such phenomenon may be attributed to the fact of poor quality of the local material. It can be assumed that the tubular shape and the raw material involved several low-quality manufacturing and conformational processes; situation that have proven to be common in the local steel markets in Colombia, due to that is highly recommended to involve always a material characterization process prior analyzing a structure.

In general, the geometry obtained using the laser scanner had minimal impact on the V&V process. The well-set parameters of the laser scanner and the control of the

scanning process variables required minimal intervention in the post-processing of the obtained mesh. This minimization reduced the uncertainty in the geometry and produced modifications or reconstructions of the numerical model that were insignificant. In addition, the final geometry of the numerical model represented the physical model to a high degree, involving only minimal modifications during the reconstruction, as surface finishing, noise cleaning, and small voids filling. This finding indicates a high level of validity. Since discrepancies in the results can be generated as a direct result of the lack of control of the geometry employed [28], the accuracy of the geometry as a software input is a key part of the verification process.

During the validation process, the photo-elastic technique proved to be a suitable tool for quantitative description of the strain distribution of the frontal plate. At the same time, this technique also proved to be sensitive to the boundary conditions and to adhesion to the plate, the latter being considered the source of error of highest impact on the results. Furthermore, the technique produced a strain pattern so mild as to require visual enhancement by increasing the vibrancy and saturation of the colors. Comparing the photo-elastic results with those in previous literature [29]–[31], the quality of the present results is comparable, and the present analysis can be regarded as successful. Moreover, we find that as an alternative for validation, photo-elastic analysis includes several susceptible stages during the validation process that may threaten or bias the process.

Although only one validation test was performed in a controlled environment, using a strain gauge and photo-elasticity simultaneously, the conditions of the test can be replicated. Moreover, all measurements were performed with calibrated equipment and high-quality commercial devices that have been used in previous FEA validation processes [32]. In order to increase its reliability for decision makers [34] and ensure complementarity, a FEA model should always include V&V processes to improve the correctness of the prediction of the physical model's response [33]. Furthermore, during the V&V processes of the computational model, verification must be performed before validation, thus enhancing the validity of the study by reducing the threat of bias.

5. CONCLUDING REMARKS

It was found that, for this specific numerical model under these loading and boundary conditions, stress and strain predictions were both below the 5% error tolerance threshold. Stress prediction was almost thirty times more accurate than strain prediction, with respective average error values of 0.13% and 3.73%. These results suggest that the V&V processes are essential for guaranteeing that the FEA can both reliably and accurately predict the mechanical response of structural models in terms of stresses, strains, and deformations.

The geometry used here faithfully represented the physical model, with a 0.338-mm average deviation between geometries. Due to the minimal uncertainty in the geometry, it was disregarded as a source of error for the model. The following potential sources of error were identified: localized changes in the behavior of the material due to welding effects and irregularities in the physical contact of the model with its boundary conditions and loads. These error sources concentrated the model's reactions atypically and modified the strain gradient.

V&V processes are needed not only to reduce the engineering risk of full-scale systems, but also to provide quantitatively support for confidence in terms of the mathematical models' safety, reliability, and performance. Decision makers' confidence in results is increased by V&V.

References

[1] Cook RD, Malkus DS, Plesha ME, Witt RJ: "Concepts and applications of finite element analysis". John Wiley & Sons, Inc.; 2007.

[2] Rodriguez JE, Medaglia AL, Casas JP: "Approximation to the optimum design of a motorcycle frame using finite element analysis and evolutionary algorithms". 2005 IEEE Design Symposium, Systems and Information Engineering 2005, 277-285.

[3] Castano MC, Zapata U, Pedroza A, Jaramillo JD, Roldan S: "Creation of a three-dimensional model of the mandible and the TMJ in vivo by means of the finite element method". International journal of computerized dentistry 2002, 5(2-3):87-99.

[4] Chung W, Sotelino ED: "Three-dimensional finite element modeling of composite girder bridges". Engineering Structures 2006, 28(1):63-71.

[5] Wang Q, Smith AL, Strait DS, Wright BW, Richmond BG, Grosse IR, Byron CD, Zapata U: "The global impact of sutures assessed in a finite element model of a macaque cranium". Anatomical record (Hoboken, NJ: 2007) 2010, 293(9):1477-1491.

[6] Goel VK, Nyman E: "Computational modeling and finite element analysis". Spine 2016, 41 Suppl 7:S6-7.

[7] Zienkiewicz OC, Taylor RL, Zhu JZ: "The finite element method: Its basis and fundamentals", 2005.

[8] Walmsley CW, McCurry MR, Clausen PD, McHenry CR: "Beware the black box: investigating the sensitivity of FEA simulations to modelling factors in comparative biomechanics". PeerJ 2013, 1:e204.

[9] Solanki KN, Horstemeyer MF, Steele WG, Hammi Y, Jordon JB: "Calibration, validation, and verification including uncertainty of a physically motivated internal state variable plasticity and damage model". International Journal of Solids and Structures 2010, 47(2):186-203.

[10] Fong JT, Marcal PV, Rainsberger R, Ma L, Heckert NA, Filliben JJ: "Finite element method solution uncertainty, asymptotic solution, and a new approach to accuracy assessment". In: ASME 2018 Verification and Validation Symposium; 2018.
[11] "Guide for verification and validation in computational solid mechanics": American Society of Mechanical Engineers-ASME; 2007.
[12] Ayturk UM, Puttlitz CM: "Parametric convergence sensitivity and validation of a finite element model of the human lumbar spine". Computational Methods Biomechanics Biomedical Egineering 2011, 14(8):695-705.
[13] Scigliano R, Scionti M, Lardeur P: "Verification, validation and variability for the vibration study of a car windscreen modeled by finite elements". Finite Elements in Analysis and Design 2011, 47(1):17-29.
[14] Oberkampf WL, Roy CJ: "Verification and validation in scientific Computing". cambridge: Cambridge University Press; 2010.
[15] Tushar M. Patel DMGBaHKP: "Analysis and validation of Eicher 11.10 chassis frame using Ansys". International journal of emerging trends and technology in computer science 2013, 2(2):85-88.
[16] Nguyen TQ: "Finite element analysis in automobile chassis design". Applied Mechanics and Materials 2019, 889:461-468.
[17] Hibbitt HD, Bhashyam GR: "Some issues associated with the validation of finite element analysis". Finite Elements in Analysis and Design 1986, 2(1):119-124.
[18] Henninger HB, Reese SP, Anderson AE, Weiss JA: "Validation of computational models in biomechanics". Proceedings of the Institution of Mechanical Engineers Part H, Journal of engineering in medicine 2010, 224(7):801-812.
[19] Várady T, Martin RR, Cox J: "Reverse engineering of geometric models—an introduction". Computer-Aided Design 1997, 29(4):255-268.
[20] Javed MA, Won SP, Khamesee MB, Melek WW, Owen W: "A laser scanning based reverse engineering system for 3D model generation". In: IECON 2013-39th Annual Conference of the IEEE Industrial Electronics Society: 10-13 2013; 4334-4339.
[21] Guo B: "Surface reconstruction: from points to splines". Computer-Aided Design 1997, 29(4):269-277.
[22] Zienkiewicz OC, Zhu JZ: "A simple error estimator and adaptive procedure for practical engineerng analysis". International Journal for Numerical Methods in Engineering 1987, 24(2):337-357.
[23] Tiossi R, de Torres EM, Rodrigues RC, Conrad HJ, de MattosMda G, Fok AS, Ribeiro RF: "Comparison of the correlation of photoelasticity and digital imaging to characterize the load transfer of implant-supported restorations". The Journal of prosthetic dentistry 2014, 112(2):276-284.
[24] Aguiar FA, Jr., Tiossi R, Macedo AP, MattosMda G, Ribeiro RF, Rodrigues RC: "Photoelastic analysis of stresses transmitted by universal cast to long abutment on implant-supported single restorations under static occlusal loads". The Journal of craniofacial surgery 2012, 23(7 Suppl 1):2019-2023.
[25] Sankararaman S, Mahadevan S: "Integration of model verification, validation, and calibration for uncertainty quantification in engineering systems". Reliability Engineering & System Safety 2015, 138:194-209.
[26] Yang X, Yan G, Xiu Y, Yang Z, Wang G, Liu W, Li S, Jiang W: "Welding temperature distribution and residual stresses in thick welded plates of SA738Gr.B through experimental measurements and finite element analysis. Materials" (Basel) 2019, 12(15):2436.
[27] Covill D, Blayden A, Coren D, Begg S: "Parametric finite element analysis of steel bicycle frames: The influence of tube selection on frame stiffness". Procedia Engineering 2015, 112:34-39.
[28] Jones AC, Wilcox RK: "Finite element analysis of the spine: Towards a framework of verification, validation and sensitivity analysis". Medical engineering & physics 2008, 30(10):1287-1304.
[29] Katanchi B, Choupani N, Khalil-Allafi J, Baghani M: "Photostress analysis of stress-induced martensite phase transformation in superelasticNiTi". Materials Science and Engineering: A 2017, 688:202-209.
[30] Ficzere P, Borbás L: "New application of 3D printing method for photostress investigation". Materials Today: Proceedings 2016, 3(4):969-972.
[31] Ficzere P, Borbas L, Szebenyi G: "Reduction possibility of residual stresses from additive manufacturing by photostress method". Materials Today: Proceedings 2017, 4(5, Part 1):5797-5802.
[32] Keyak JH, Fourkas MG, Meagher JM, Skinner HB: "Validation of an automated method of three-dimensional finite element modelling of bone". Journal of Biomedical Engineering 1993, 15(6):505-509.
[33] Thacker BH, Doebling SW, Hemez FM, Anderson MC, Pepin JE, Rodriguez EA: "Concepts of model verification and validation". In. Edited by (US) UD: Los Alamos National Lab., Los Alamos, NM (US); 2004.
[34] Roy CJ, Oberkampf WL: "A comprehensive framework for verification, validation, and uncertainty quantification in scientific computing". Computer Methods in Applied Mechanics and Engineering 2011, 200(25):2131-2144.

AUTHOR

Carlos Urrego M.Sc. received a B.S. in Mechanical Engineering and a M.S. degree in Engineering from Universidad EAFIT (Medellín, Colombia) in2018 and 2019, respectively. During 2018-2020, he researchedat theMaterials in Engineering Research Laboratory (GME), in Universidad EAFIT; dedicating his work to the structure analysis and materials characterization.

Uriel ZapataPh.D. M.Sc. Professor at Eafit University. Researcher on applications of finite element method and biomechanics. Receivedresearch awards from Fulbright, Matsumae International Foundation, and National Science Foundation. Published several manuscripts associated with Finite Element Analysis and biomaterials.